

Flexural behavior of singly curved GFRP sandwich panel with polyurethane foam core

Xinmiao Meng^{a,*}, Daobo Zhang^b, Peng Feng^{b,*}, JiaQi Zhai^c, TianQiao Liu^d

^a Department of Civil Engineering, Beijing Forestry University, Beijing 100083, China

^b Department of Civil Engineering, Tsinghua University, Beijing 100084, China

^c Sinoma Wind Power Blade Co., Ltd., Beijing 100192, China

^d Department of Civil Engineering, Beijing University of Technology, Beijing 100124, China

ARTICLE INFO

Keywords:

Fiber-reinforced polymer
Sandwich arch
Flexural test
Parametric study
Failure mechanism

ABSTRACT

Curvilinear architecture and structures are becoming a worldwide trend for its streamlined appearance and synchronicity with the surroundings. Nonetheless, the conventional construction materials might not be able to achieve the desired curvilinear geometries in an effective and economic manner. In this regard, glass fiber-reinforced polymer (GFRP) curved sandwich panel with polyurethane foam core is able to meet the requirement of the construction efficiency and economy as well as satisfy the need for a lower energy consumption. However, few studies are available on the mechanical behavior of such panels. In this regard, this work was to conduct an experimental and numerical investigation on the singly curved GFRP sandwich panels to evaluate the flexural performance. In particular, the effect of the foam density, inclined angle, core thickness and stacking sequence of face sheet on the load-carrying capacity and failure mode was addressed. Four failure modes were identified. The singly curved GFRP sandwich panel showed an improved stiffness when compared to the flat panel, but showed more complicated failure mechanism. The stiffness of the curved panel with inclined angle 30° was 250 % higher than that of the flat panel in the test results. It was shown that the strength and stiffness increased as the density and thickness of the foam core increased. In addition, a finite element analysis was conducted via MSC.Marc and validated by the experimental results. A parametric study was performed to address the design parameters. It was found that the specimens with inclined angles of 30° and 45° showed the greatest stiffness.

1. Introduction

Curvilinear architecture has seen a rapid development in recent years [1]. It releases the imagination and creation of architects in designing new buildings and infrastructures [2]. In this regard, the new construction technology finds its opportunity in an increasing number of modern structures. This is primarily due to the fact that the conventional construction techniques are often based on a formwork system and thus, have difficulty in constructing the free-form appearance with acceptable cost in terms of the time and effort [3]. In addition to the cost consideration, the thermal performance needs to be particularly concerned, as the modern curvilinear buildings often come with a higher energy consumption due to their relatively complex architectural geometry [4]. Thus, customized thermal insulation is typically needed, and it has become one of the most important measures of the overall thermal

performance of the building envelope. Nonetheless, conventional thermal insulation approaches, such as the concrete sandwich panels [5] and the exteriorly insulated walls [6], are relatively complex in details and might result in a low efficiency in the construction of curvilinear architectures.

Curved fiber reinforced polymer (FRP) sandwich panel, consisting of FRP face sheets and polyurethane (PU) foam core, provides an effective solution to the aforementioned cost-efficiency and thermal performance [7]. For instance, curved glass fiber-reinforced polymer (GFRP) sandwich panels have been adopted as an esthetical envelope of the Tongzhou bridge in Beijing, China (Fig. 1a) [8], the shell of the wind turbine blade (see Fig. 1b) [9] and the floating and stationary facilities in bridge anti-collision application [10]. FRP material is widely known to have a low density, high strength, ease of construction and excellent designability [11,12]. In addition, PU foam has a low thermal conductivity

* Corresponding authors.

E-mail addresses: mengxinmiao@bjfu.edu.cn (X. Meng), fengpeng@tsinghua.edu.cn (P. Feng).

<https://doi.org/10.1016/j.engstruct.2024.118389>

Received 4 December 2023; Received in revised form 11 May 2024; Accepted 5 June 2024

Available online 12 June 2024

0141-0296/© 2024 Elsevier Ltd. All rights reserved, including those for text and data mining, AI training, and similar technologies.

and has been widely used as a thermal insulation material. The proposed panel in this work combines the advantages of both FRP and PU foam and thus, is able to realize the rapid construction and achieve the excellent thermal performance [13,14]. Several pioneering curvilinear architectures have been constructed worldwide [15–17], such as Hoofddorp bus station (Netherlands) [18], Yitzhak Rabin center (Israel) [19], Novartis main gate building (Switzerland) [20,21], Wuhan factory gate building (China) [22] and Beijing bridge enclosure (China) [23].

Nonetheless, existing research was mainly focused on the curved FRP sandwich panels with rigid core, and few studies investigated the static behavior. In particular, many scholars from the aerospace industry have focused on the vibration behavior [24–27]. On the other hand, some experimental and numerical studies focused on the extreme events such as the blast loading [28–35]. As aforementioned, the thermal performance is an essential factor in the design of curved sandwich panels, and this is true for both the aerospace and civil industries [36–38]. In addition, the static behavior, especially buckling performance of curved sandwich panels were evaluated by few scholars. Frostig et al. [39] proposed a high-order theory for sandwich-beam behavior with transversely flexible core. Skvortsov and Bozhevolnaya [40–42] assessed the existing theoretic models for singly-curved sandwich panels under static loads, and they proposed a new model to predict the overall static behavior of the panel. Afshin et al. [43] investigated the static response of cylindrical sandwich panels with flexible core based on the high-order theory of sandwich structures. Pope et al. [44] and Davenport et al. [45], on the other hand, studied the buckling characteristics of isotropic and orthotropic curved sandwich panel under the combination of axial compression and shear. Hause et al. [46] conducted a theoretical study on the post-buckling behavior of geometrically imperfect anisotropic doubly-curved sandwich panels subjected to various loading condition. Gao et al. [47], Hosseini et al. [48] and Kundu et al. [49] also carried out buckling analysis on curved composite sandwich panels via finite element method. It is identified that in many scenarios the concentrated load is the most detrimental loading condition for curved FRP sandwich panels with soft core or truss core. However, few studies have focused on the concentrated loads. Xiong et al. [50] conducted experimental and numerical studies on the flexural behavior of a composite curved panel with pyramidal metallic truss core. Xie et al. [51,52] investigated the flexural behavior and failure mechanisms of curved sandwich beams with polyethylene terephthalate (PET) foam. The effects of thickness and curvature radius were evaluated, and the results showed that the ultimate load-bearing capacity and stiffness of the CSBs decreased by 17.7 % and 61.8 % as the curvature decreased from 1150 to 300 mm. In addition, as for the flat FRP sandwich panel with foam core, four failure modes have been identified in previous research [53], whereas the failure modes of the curved panels with foam core still needed more investigation.

In order to investigate the flexural performance of the curved sandwich panel with foam core as well as to augment the data for the field, a

series of three-point bending tests under concentrated loads were conducted on the singly curved sandwich panels. Moreover, the influences of different geometrical and physical parameters on the load capacity and failure modes of the panels are addressed. In addition, a finite element analysis was conducted via MSC.Marc to reveal the damage progress and to perform the parametric study.

2. Experimental program

2.1. Material properties

In this work, the singly curved sandwich panels consist of GFRP face sheets and PU foam core. The glass fiber sheets were HITECH-G430S unidirectional fabric with density of 430 g/m^2 , and were manufactured by Nanjing Hitech Composites Co., Ltd. The resin system was SWANCOR 2511-1A/BS epoxy resin and produced by Swancor (Tianjin) Wind Blade Materials Co., Ltd. The PU foam was closed-cell and produced by Kezhao New Materials Co., Ltd. The GFRP face sheets were manufactured through vacuum-assisted resin transfer molding (VARTM) process and computer numerical control (CNC) machining, as shown in Fig. 2.

The thickness of one single layer of GFRP face sheets (after molding) was approximately 0.45 mm, and the fiber volume fraction was approximately 37.6 %. The tensile, compressive and shear properties were assessed according to Chinese standards GB/T 1447-2005, GB/T 1448-2005, GB/T 3355-2014, respectively. Each test was performed on five coupons and the results are shown in Table 1. The coupons were prepared through VARTM process and CNC machining. The sizes of the coupons were $250 \times 25 \times 2.4 \text{ mm}$ in tensile tests, and $250 \times 25 \times 2.9 \text{ mm}$ in shear tests. In order to avoid the buckling failure, the sizes of the coupons in compressive tests were $10 \times 10 \times 2.4 \text{ mm}$ in 0° direction and $10 \times 6 \times 2.4 \text{ mm}$ in 90° direction. The loading rate was 2 mm/min for each test. The GFRP sheets showed a linear elastic behavior until failure under compression and tension. The material properties of PU foam core are shown in Table 2. The stress-strain relationships of PU foam coupons are shown in Fig. 3. It could be seen that the strength and modulus increased as the density increased. It could also be found that for PU foam the compressive strength was not equal to the tensile strength, and the compressive stress-strain relationship had a relatively longer yield plateau, as shown in Fig. 3(a). In addition, the tensile failure of PU was brittle, as shown in Fig. 3(b), and the shear failure became brittle when the density was greater than 77.6 kg/m^3 , as shown in Fig. 3(c). It is worth noting that the PU foam with density of 77.6 kg/m^3 exhibited a nonlinear behavior in the shear test.

2.2. Specimen design

A total of eleven singly-curved sandwich panels were manufactured, and also, one flat sandwich panel was made for comparison purpose, as



Fig. 1. Curved GFRP sandwich panels as (a) the envelope of a bridge (Beijing, China) and (b) the shell of the wind blade.



Fig. 2. Manufacture process of singly curved GFRP sandwich panel with foam core: (a) VARTM process and (b) CNC machining.

Table 1
Mechanical properties of GFRP sheets.

Tension 0°		90°		Compression 0°		90°		Shear ± 45°	
E_{Lt} (GPa)	F_{Lt} (MPa)	E_{Tt} (GPa)	F_{Tt} (MPa)	E_{Lc} (GPa)	F_{Lc} (MPa)	E_{Tc} (GPa)	F_{Tc} (MPa)	G_{LT} (GPa)	F_{LT} (MPa)
38.9 (2.0 %)	773 (2.1 %)	10.6 (3.7 %)	27.2 (4.4 %)	38.1 (3.1 %)	220.1 (6.0 %)	11.2 (4.6 %)	95.8 (4.9 %)	3.29 (3.6 %)	45.7 (3.9 %)

Note: The value in the parentheses represents the coefficient of variation.

Table 2
Mechanical properties of PU foam core.

Density designation	Density (kg/m ³)	Tension		Compression		Shear	
		E_t (MPa)	F_t (MPa)	E_c (MPa)	F_c (MPa)	G (MPa)	F_u (MPa)
D1	53.6 (1.02 %)	5.93 (2.36 %)	0.27 (5.56 %)	4.88 (1.33 %)	0.24 (5.42 %)	2.18 (3.30 %)	0.21 (5.71 %)
D2	77.6 (0.71 %)	12.52 (2.80 %)	0.58 (4.83 %)	11.34 (1.15 %)	0.50 (4.20 %)	4.96 (3.43 %)	0.3 (5.00 %)
D3	125.6 (0.44 %)	28.19 (1.92 %)	0.84 (4.40 %)	27.54 (1.05 %)	1.23 (2.36 %)	12.68 (2.76 %)	0.47 (4.47 %)
D4	168.5 (0.42 %)	43.16 (2.83 %)	1.30 (5.46 %)	47.96 (1.42 %)	2.23 (2.87 %)	20.81 (2.93 %)	0.65 (5.54 %)
D5	211.0 (0.89 %)	60.75 (3.34 %)	1.92 (5.73 %)	68.39 (1.93 %)	3.44 (2.70 %)	28.55 (2.94 %)	0.86 (5.47 %)

Note: The value in the parentheses represents the coefficient of variation.

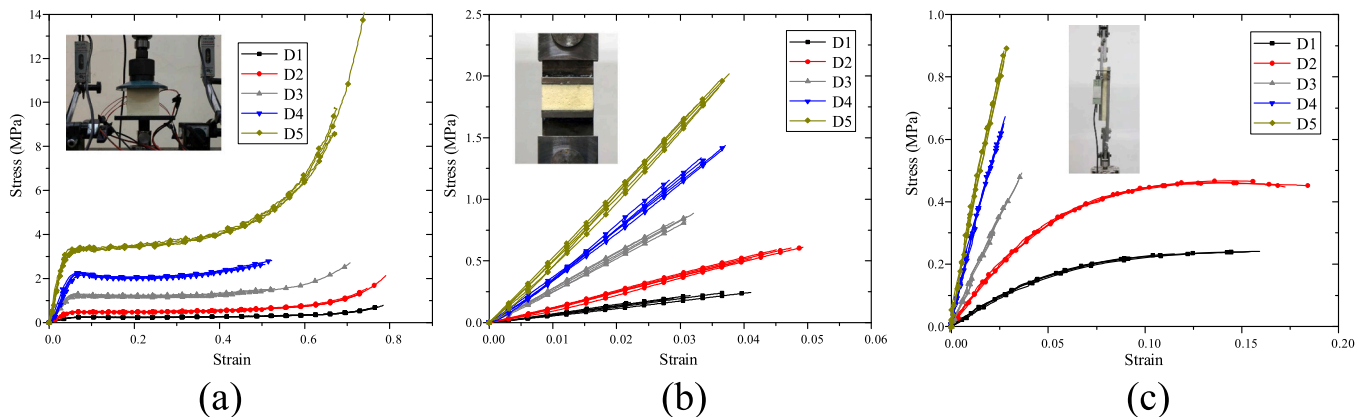


Fig. 3. Experimentally determined stress-strain relationships of PU foam: (a) compression, (b) tension and (c) shear tests.

shown in Table 3. The foam density, inclined angle, core thickness and stacking sequence of face sheet were considered in the specimen design, including five densities, four inclined angles, two foam thicknesses and four stacking sequences. Therefore, the specimen was designated as follows (taking D1-30-20-A as an example): the first part D1 represents

the density of PU foam core (see Table 2); the second part 30 indicates the inclined degree of the panel; the third part 20 represents the thickness of the PU foam core; and the last part A is the stacking sequence of GFRP face sheet (0° indicates that the fiber is parallel to the longitudinal direction of the specimen). The fiber in 90° direction is designed to

Table 3
Details of the specimens.

Specimens	Foam density (kg/m ³)	Inclined angle (°)	Thickness of the core h_c (mm)	Stacking sequence (°)
D1-30-20-A	53.6	30	20	0/90/0
D2-30-20-A	77.6	30	20	0/90/0
D3-30-20-A	125.6	30	20	0/90/0
D4-30-20-A	168.5	30	20	0/90/0
D5-30-20-A	211.0	30	20	0/90/0
D3-00-20-A	125.6	0	20	0/90/0
D3-60-20-A	125.6	60	20	0/90/0
D3-90-20-A	125.6	90	20	0/90/0
D3-30-15-A	125.6	30	15	0/90/0
D3-30-20-B	125.6	30	20	0
D3-30-20-C	125.6	30	20	0/90/0/90/0
D3-30-20-D	125.6	30	20	0/0/90/0/0

prevent the splitting failure of the GFRP face sheet. In the four stacking sequences, the longitudinal layer increases from one layer to four layers individually. The thickness of face sheet can be estimated based on the thickness of one single layer. The schematic diagram of the specimens is shown in Fig. 4. More detailed information of each specimen is presented in Table 3.

2.3. Experimental setup and instrumentation

The test setup is shown in Fig. 5(a). In order to realize the arch structure, the translation degree of the support should be restricted. In addition, the rotation degree was also restricted. Since all the specimens were thin panels with low bending rigidity, the rotation constraint would show less influence on the failure mechanism compared to that of releasing the rotation constraint when subjected to the concentrated load. The specimen ends were first glued to steel plates to adequately fix the two ends of the panel, and then the steel plates were bolted at the foundation, as shown in Fig. 5(b). Three linear variable displacement transducers (LVDTs) were installed to measure the overall and the local compressive deformations of the panel, and twelve strain gauges were installed on the top and bottom GFRP face sheets (six at each side), as shown in Fig. 5(c). The loading was applied in the manner of displacement-control, and the loading rate was 1 mm/min.

3. Experimental results

3.1. Experimental observations and failure modes

Four types of local damages were observed during the tests, including core shear (CS) crack, face crushing (FC), face wrinkle (FW) and indentation (INT), as shown in Fig. 6. Furthermore, four failure

modes of the singly curved sandwich panel with foam core were identified and shown in Table 4: (I) Failure mode CS, in which pure shear crack of PU core occurred without causing other damages; (II) Failure mode FC-INT-CS, in which face sheet showed compressive failure first, and then indentation and core shear crack occurred; (III) Failure mode INT-CS, in which indentation occurred first and finally core shear crack occurred; (IV) Failure mode INT-FW-CS, in which indentation occurred first and then face sheet wrinkled, and finally the core cracked due to shear.

The failure mode CS was observed for the specimens D1-30-20-A, D3-60-20-A, D3-90-20-A, D3-30-15-A, D3-30-20-C and D3-30-20-D. In this mode, the PU foam core under the loading roller did not exhibit a significant deformation during the loading process, and when the maximum load was reached, the PU core suddenly shear-cracked and the load sharply decreased. The top and bottom FRP face sheets were then separated by the diagonal shear crack. The failure mode CS showed to be sudden and brittle.

The failure mode FC-INT-CS was seen during the loading process of specimens D3-00-20-A, D3-30-20-A and D4-30-20-A. In this mode, the localized compressive deformation of the PU foam core under the loading roller was not significant during the initial loading stage. However, the indentations occurred and rapidly developed when reaching the maximum load. At the maximum load, the face sheets under the loading roller yielded and the capacity of the panel decreased. For specimen D3-00-20-A, a plastic hinge at the midspan was formed and consequently, the stress flow in the panel transitioned from that of a beam system to that of a catenary system, and the bottom face sheet started to carry tensile force. For the other two specimens D3-30-20-A and D4-30-20-A, the PU core showed shear crack right after the face yielded and the capacity decreased.

The failure mode INT-CS was only observed for specimen D2-30-20-A. When the load reached $0.9P_{max}$ (P_{max} is the maximum load), the indentation rapidly developed and the load gradually increased. After a large indentation occurred under the loading roller and a significant deformation was seen for the entire sandwich panel, the core shear crack suddenly occurred and the capacity dramatically decreased.

The failure mode INT-FW-CS was observed for specimens D3-30-20-B and D5-30-20-A. During the initial loading process, no local deformation was observed under the loading roller. When the load reached $0.6P_{max}$, the indentation started to form and gradually developed. When the maximum load was reached, the top face sheet near the loading roller wrinkled and the capacity slightly decreased. Finally, the shear crack of PU core occurred, leading to a sudden drop of the load.

In addition, some experimental phenomena were observed during the tests. First, the PU foam exhibited an intensive and slight sound when approaching the failure load. Second, the panel was able to hold the load at a low level after the core shear occurred. Finally, most of the deformation can be recovered when uploading the panel, since the bottom GFRP face sheet was still in a good condition.

3.2. Load-displacement relationships

3.2.1. Load-displacement relationships at midspan

The load-displacement curve was obtained through the displacement transducer placed at the top face sheet at the midspan. A total of eleven load-displacement curves were obtained and can be categorized into four groups with respect to the four failure modes, as shown in Fig. 7.

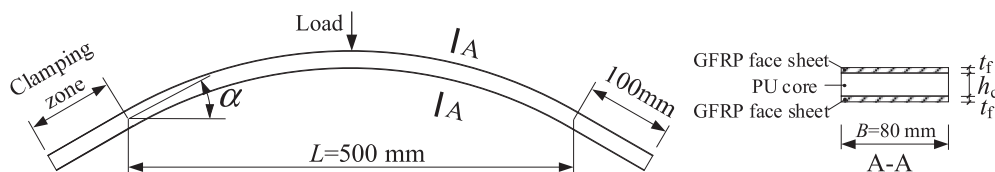


Fig. 4. Schematic diagram of singly curved GFRP sandwich panel.

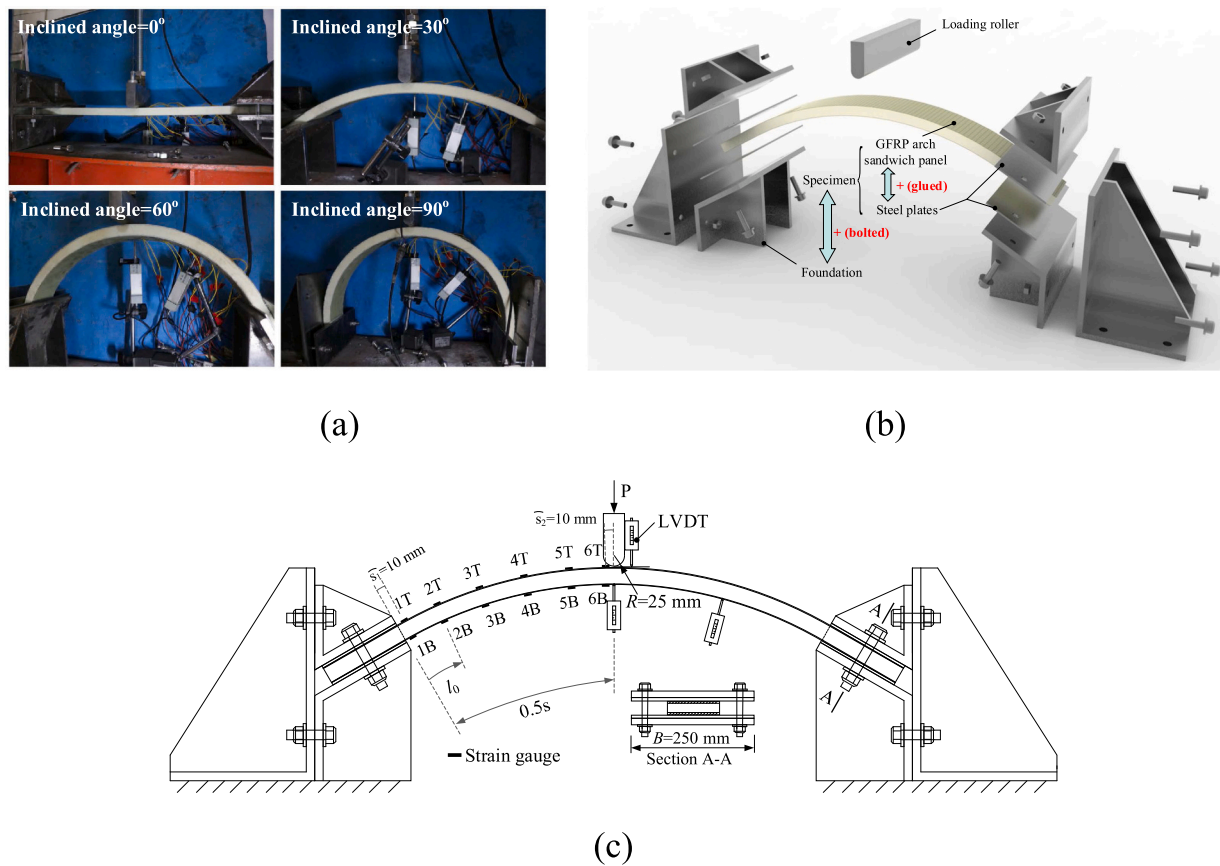


Fig. 5. Experimental setup and instrumentation: (a) overall view, (b) schematic view, and (c) layout of the LVDTs and strain gauges.

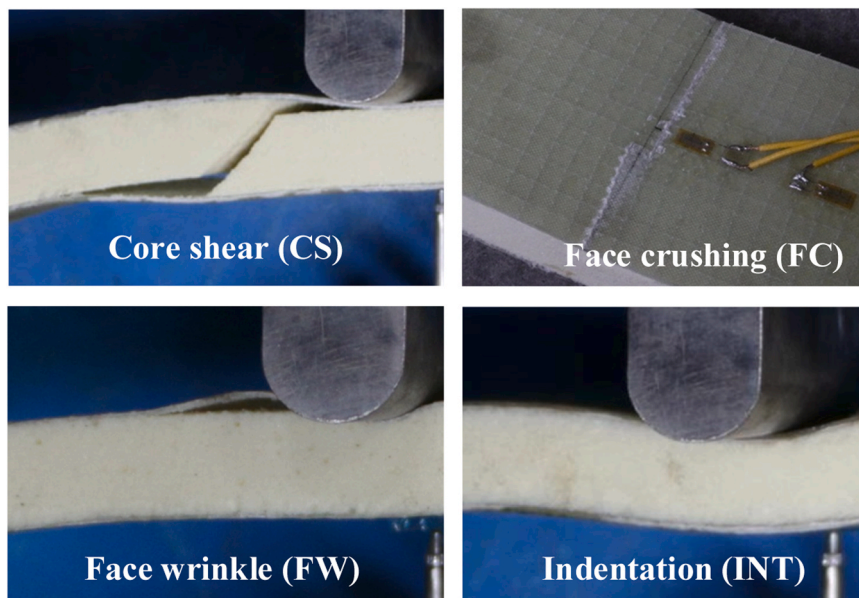


Fig. 6. Four types of damages of specimens.

Detailed experimental results are summarized in Table 4. The initial stiffness of panels was evaluated using the tangent of the linear stage.

Fig. 7(a) shows the load-displacement curves of failure mode CS. The load-displacement relationships were linear at the beginning. As the load increased, the stiffness of the panel slightly decreased when the foam core developed into its plastic zone. Additionally, the large displacement might also result in a reduced stiffness. It is seen that the

load suddenly dropped to a great amount, when the shear crack of PU core occurred. After that, the load was shown to slightly increase as the top and bottom face sheets were still partially connected to each other by the residual part of the core.

Fig. 7(b) shows the load-displacement curves of failure mode FC-INT-CS. The curves were linear at the beginning, and then, a slight stiffness-soften segment could be seen. Due to the local stress concentration, top

Table 4
Experimental results of the specimens.

Specimens	Initial stiffness (kN/mm)	Maximum load (kN)	Failure mode
D1-30-20-A	0.141	0.567	CS
D2-30-20-A	0.301	1.260	INT-CS
D3-30-20-A	0.564	2.195	FC-INT-CS
D4-30-20-A	0.819	3.512	FC-INT-CS
D5-30-20-A	0.994	3.968	INT-FW-CS
D3-00-20-A	0.159	6.065	FC-INT-CS
D3-60-20-A	0.503	2.176	CS
D3-90-20-A	0.323	2.210	CS
D3-30-15-A	0.472	1.689	CS
D3-30-20-B	0.424	1.295	INT-FW-CS
D3-30-20-C	0.716	2.505	CS
D3-30-20-D	0.767	3.040	CS

face sheet near the loading roller was compressed to the crushing failure and turned into white color, and the stiffness saw a relatively large decrease. When approaching the maximum load, the face sheets under the roller indented and the load showed a slight drop. For the curved sandwich panels, the core shear crack took place soon after the indentation. However, for the flat sandwich panel, the load continued to increase while showing a comparable stiffness to that of the linear stage. This is due to the formation of the plastic hinge at the midspan, that is,

the structure transitioned from a beam system into a catenary system.

Fig. 7(c) shows the load-displacement curve of failure mode INT-CS. It consists of four segments, including linear, stiffness-soften, plateau and core shear crack segments. The stiffness-soften segment resulted from the development of plastic zone of the foam core and the large displacement. When the load approached the maximum, the indentation took place. Then, the capacity was able to hold until the core shear crack occurred. In the plateau segment, an evident indentation and a large vertical displacement of the panel were observed.

Fig. 7(d) shows the load-displacement curves of failure mode INT-FW-CS. The curves were similar to other failure modes in the linear and stiffness-soften segments. However, the FRP face sheets showed a considerable indentation. After that, the face wrinkle occurred near the loading roller. The capacity had a slight drop for specimen D3-30-20-B when the face wrinkled. Then, the load dramatically dropped when the core was shear-cracked. Similar to other failure modes, the capacity was not totally lost after the shear crack of core occurred.

3.2.2. Load-compression relationships at midspan

The load-local compression relationships of specimens are shown in Fig. 8. These local compressions were calculated from the measured differences between the top and bottom displacement transducers. The failure process of the panel as well as the local damage of the indentation

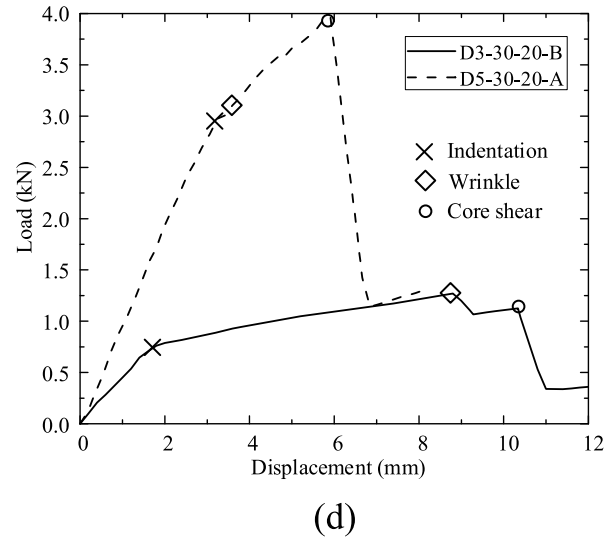
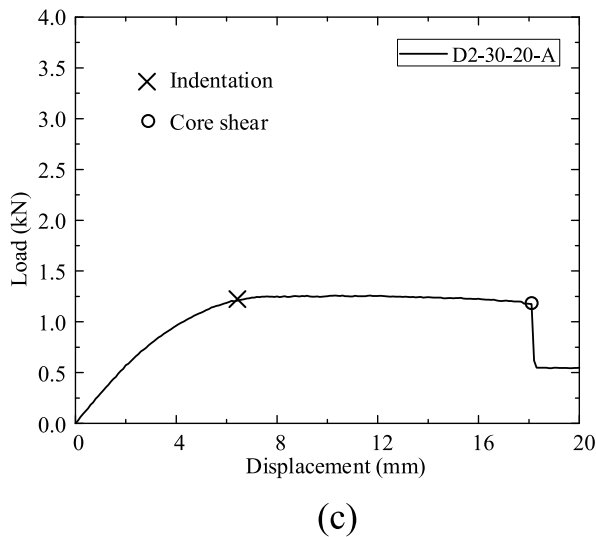
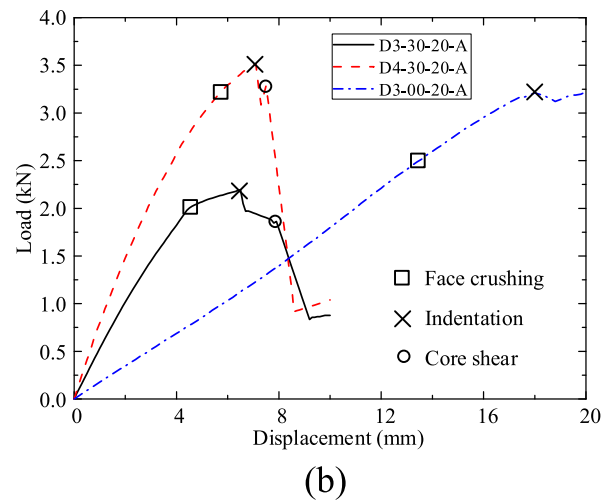
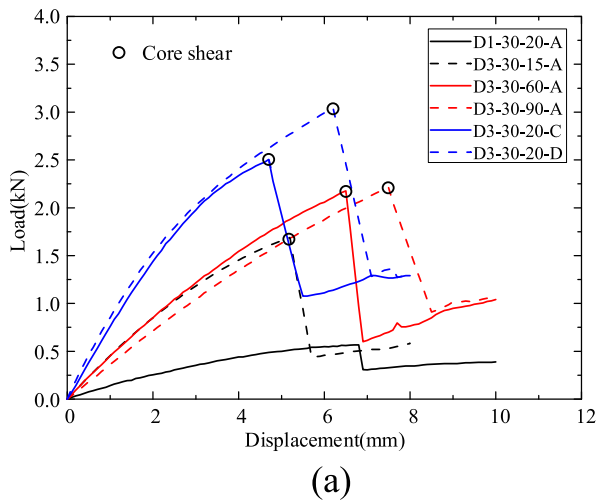


Fig. 7. Load-displacement curves at midspan of specimens: (a) failure mode CS, (b) failure mode FC-INT-CS, (c) failure mode INT-CS and (d) failure mode INT-FW-CS.

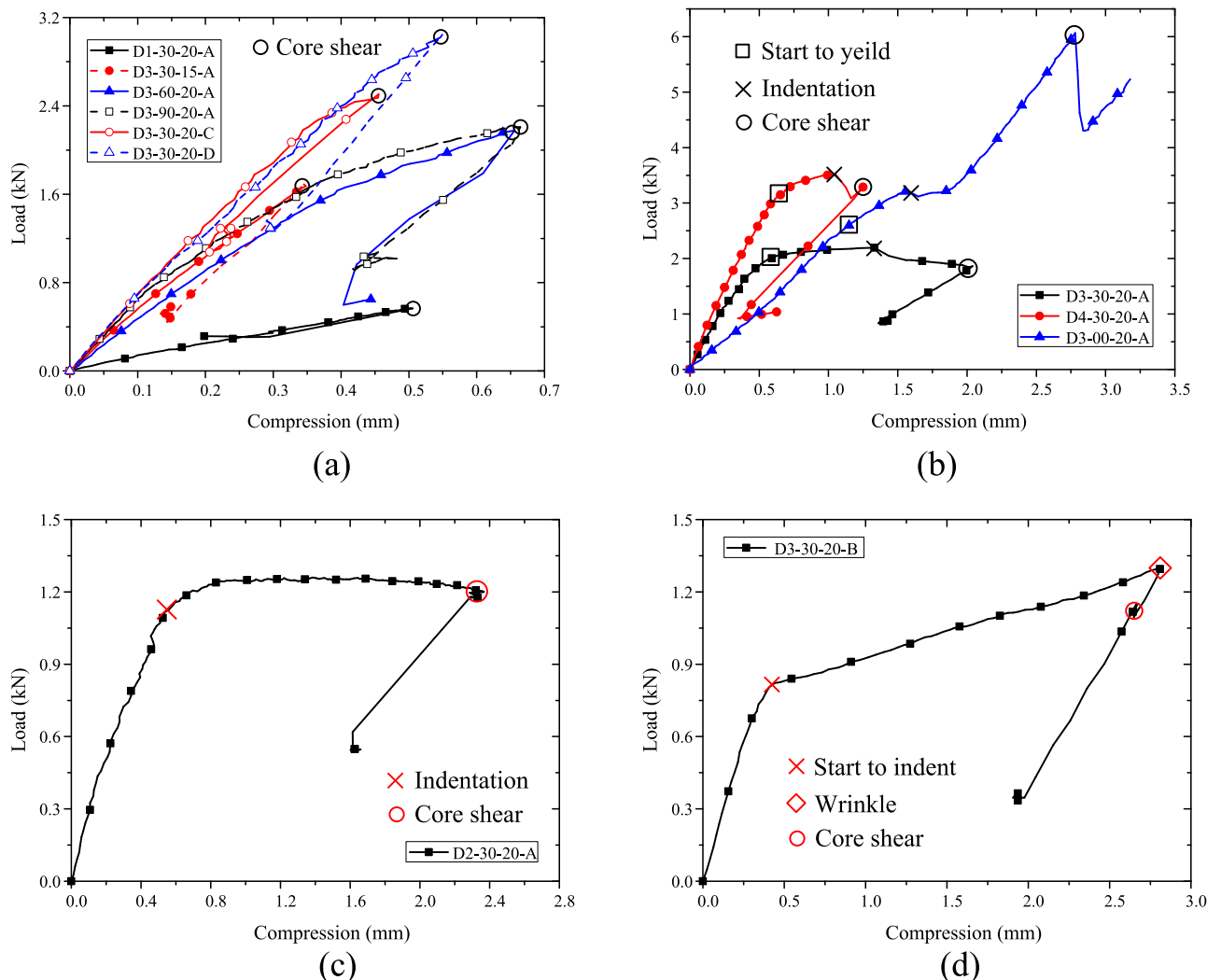


Fig. 8. Load-compression curves at midspan of specimens: (a) failure mode CS, (b) failure mode FC-INT-CS, (c) failure mode INT-CS and (d) failure mode INT-FW-CS.

can be identified from the local compression.

Failure mode CS is featured by the core shear crack, and thus, the local compression at the loading roller was not evident. This is validated by the maximum compression of specimen D1-30-20-A whose measured compression was less than 0.7 mm, as shown in Fig. 8(a). In addition, the local compression was able to recover after the core shear crack. Failure mode FC-INT-CS consists of the face yield and indentation. The local compression, therefore, increased dramatically when the face sheets started to yield, as shown in Fig. 8(b). When indentation occurred, the load had a drop, while the local compression continued to increase until the core was shear-cracked. However, residual deformation existed for this type of failure mode. Failure modes C and D both showed an evident indentation, as shown in Figs. 8(c) and 8(d), and the local compression and the residual deformation were larger than those of other failure modes.

In conclusion, the specimens with the face sheets having relatively low stiffness or damage, showed a remarkable local compression due to the stress concentration at the loading roller. Therefore, the deformations of the top and bottom face sheets were not the same. In this regard, a unified function may not be feasible in defining the deformed geometries of the panels.

3.3. Load-strain response

The load-strain relationships of specimens having different inclined

angles are shown in Fig. 9. Since the damage mainly occurred at the top face sheet, the load-strain relationships obtained from the top face sheet are reported and discussed.

For failure mode CS, FRP face sheets did not show any damages other than the core shear crack. The vertical deformation and local compression of the panel were limited, and the curves are almost linear until failure, as shown in Fig. 9(a). For failure mode FC-INT-CS, the face sheets near the loading roller yielded and damaged. After the indentation, the face sheets near the loading roller started to carry tensile force, as shown by the strain readings in Fig. 9(b). For failure mode INT-CS, the load-strain relationship is shown in Fig. 9(c). It can be found that the initial curve was almost linear until the indentation occurred. Since the density of the foam core of specimen D2-30-20-A was low, its modulus and strength were small. Therefore, the stiffness ratio of GFRP face sheets to the PU foam core was relatively large. After the indentation, the vertical deformation of the panel was large due to the low shear modulus of the foam core. Moreover, the area of the indentation was larger than that of failure mode FC-INT-CS. Strain gauge 6 T was located closest to the loading roller and its reading continued increasing after the indentation, while the other strains, measured by strain gauges 1–5 T, turned into tensile strains. For failure mode INT-FW-CS, the load-strain relationship of specimen D3-30-20-B is shown in Fig. 9(d). Due to the thin GFRP face sheet (having only one layer of fabric), the stiffness ratio of face sheets to the foam core was relatively low, and the area of indentation was limited to the loading roller. The

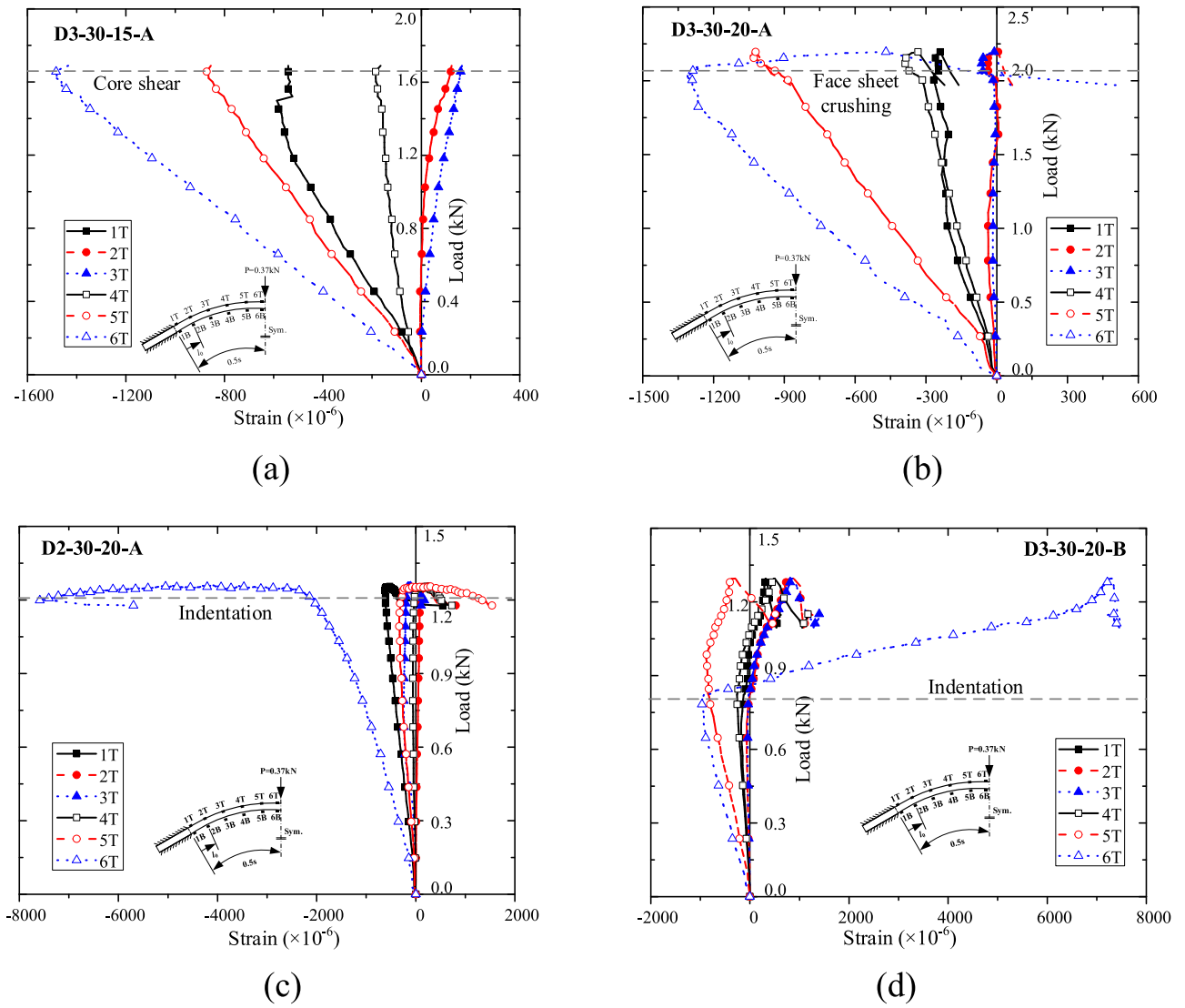


Fig. 9. Load-strain curves of specimens: (a) failure mode CS, (b) failure mode FC-INT-CS, (c) failure mode INT-CS and (d) failure mode INT-FW-CS.

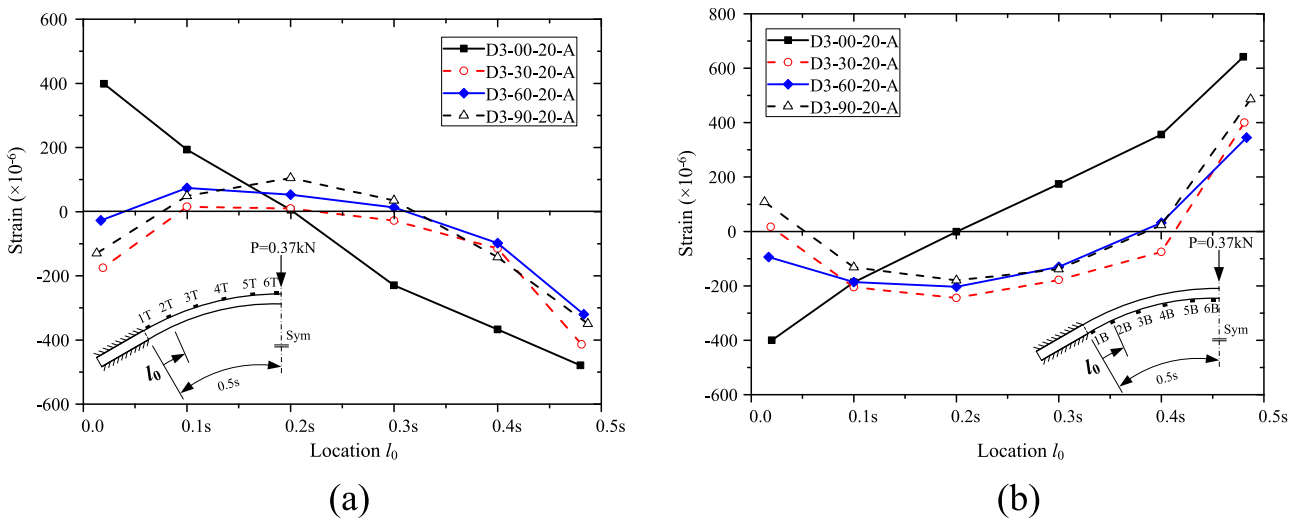


Fig. 10. Strain distributions of specimens with different inclined degrees: (a) upper face sheets and (b) lower face sheets.

strain gauge 6 T was located at the edge of the indentation region, and thus, its strain reading changed from compressive to tensile as the indentation occurred. The other strains gradually turned into tensile strains due to the large vertical deformation of the curved sandwich panel.

3.4. Strain distribution

Typically, for the proposed curved sandwich panel the top and bottom face sheets are to carry compression and tension, while the core is to sustain the shear force. Nonetheless, different geometries may result in different stress and strain distributions. To study and compare the strain distributions of each specimen, the load P of 0.37 kN was selected for all specimens, as they were all in the linear stage.

The strain distribution curves of specimens having different inclined angles are shown in Fig. 10. For curved specimens, the strain distributions were similar to each other and due to the arch effect, axial forces are generated at the ends. However, for flat panel, no axial force was provided, and the tension and compression in the top and bottom face sheets of flat panel only resulted from the bending moment, and were equal in magnitude and opposite in directions, as shown in Figs. 10(a) and 10(b). For the curved panels, the axial forces existed due to the arch effects, and thus, the axial forces, tension and compression, in top and bottom face sheets resulted from both the axial forces applied at the ends and the bending moments due to the concentrated load. Thus, the strain

distributions of the curved panels were different from the flat ones. Additionally, the strain distributions of all curved panels are in a similar form, while the magnitudes are different due to the different geometries and physical parameters of all specimens.

4. Analysis and discussion

4.1. Failure modes

The four failure modes consisted of one or more local damages, of which the core shear crack was the most common one. When loading the specimens to their ultimate failures, the core shear crack always occurred with a sudden drop of the load. The indentation was another common damage observed in the tests. A stress concentration was produced under the loading roller, leading to indentation through the plastic compressive deformation of the foam core and local flexural deformation of the face sheets. The indentation is to be avoided for the sandwich structures in practical applications. The face crushing was failure mode in strength limit state, which was caused by the compressive axial force in the top face sheet and the concentrated load. The face wrinkle occurred after a large indentation. The separate location of the wrinkle was in the core, while not at the border between the core and the top face sheet as the strength of the core was less than that of the glue polymer.

In addition, the effects of design parameters were discussed. First, the

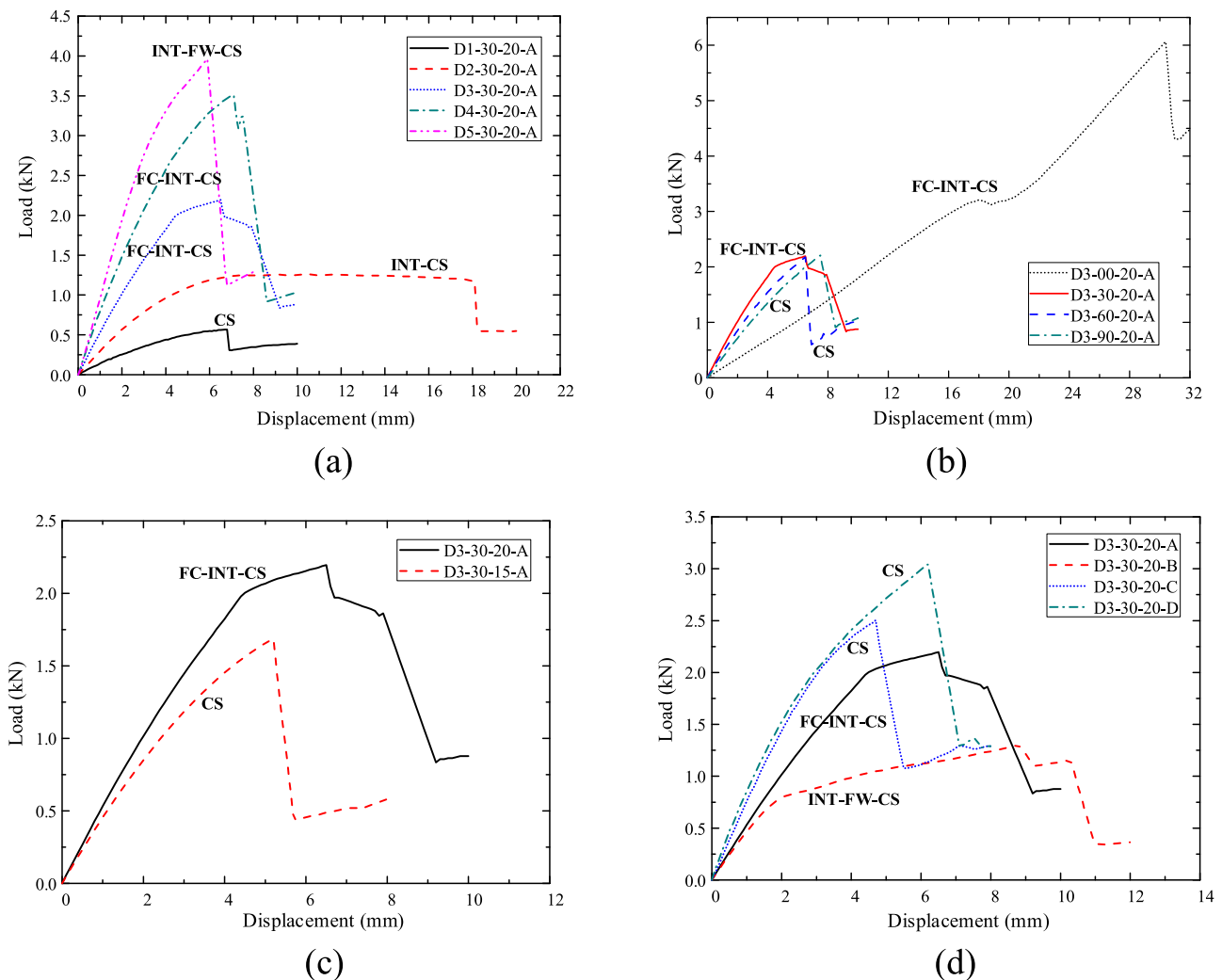
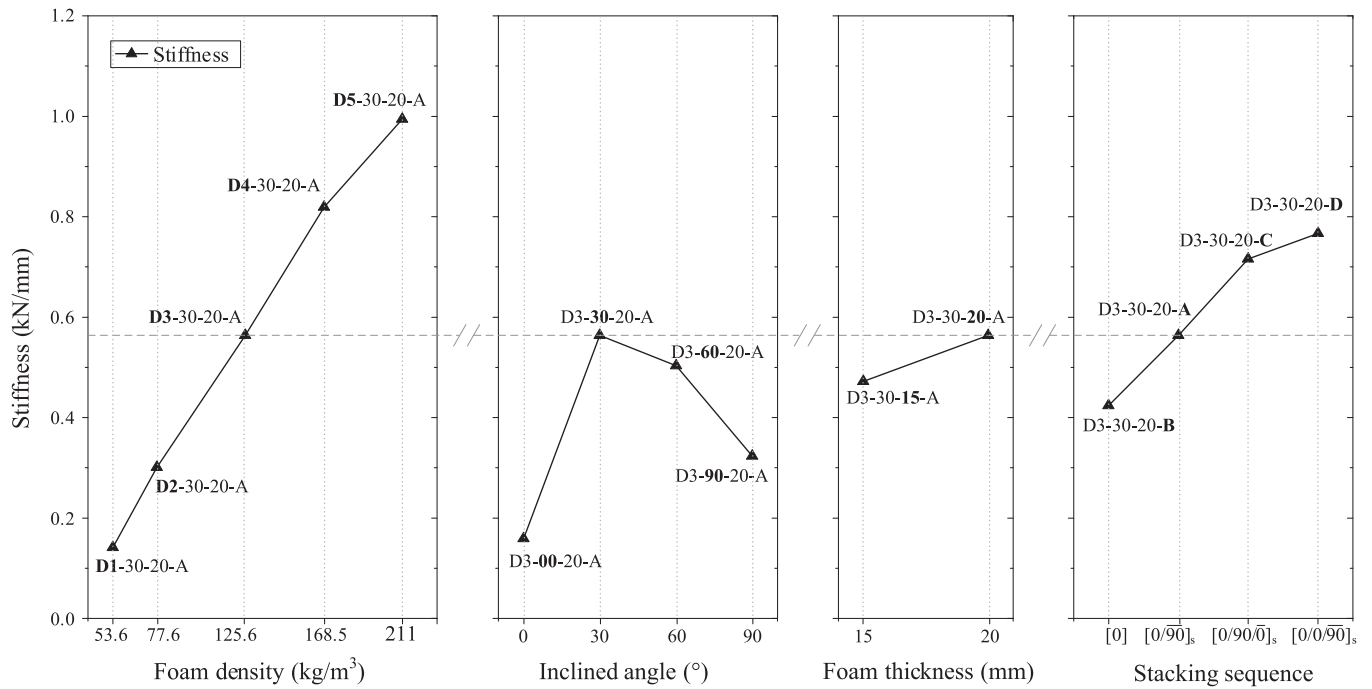


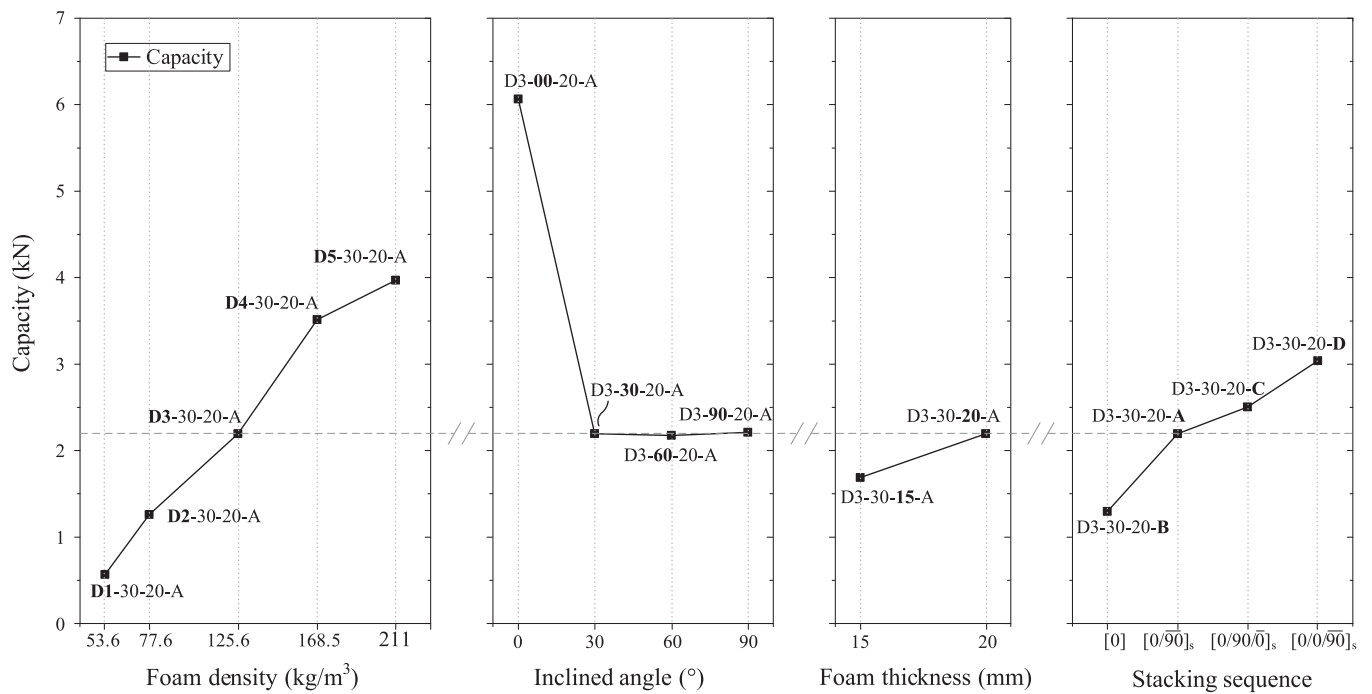
Fig. 11. Comparisons of load-displacement curves at midspan influenced by design parameters: (a) foam density, (b) inclined angle, (c) core thickness and (d) stacking sequence of face sheet.

foam density is related to the strength and modulus. When the foam density increased, the strength and modulus of the sandwich core increased and the failure modes changed from CS to FC-INT-CS, as shown in Fig. 11(a). Second, the inclined angle influenced the stress distribution. The failure modes changed from FC-INT-CS to CS as the inclined degree increased, as shown in Fig. 11(b). Third, the sandwich core is to carry the shear force and contributes to the shear deformation of the overall deformation. When the thickness of the core increased, the

failure modes changed from CS to FC-INT-CS, as shown in Fig. 11(c). Finally, the stacking sequence, particularly those layers in 0° direction, had a great influence on the local deformation. When the layers in 0° direction increased, the failure modes changed from INT-FW-CS to FC-INT-CS and then to CS, as shown in Fig. 11(d).



(a)



(b)

Fig. 12. Mechanical behavior influenced by design parameters: (a) initial stiffness and (b) load-carrying capacity.

4.2. Stiffness and capacity

The capacity and stiffness of the panel are summarized in Table 4. As for the capacity, it could be found that the maximum load of panel was determined by the failure mode. If the failure mode was core shear, the capacity is to be predicted by the shear strength of foam core and the shear contribution from GFRP face sheets. However, if the other failure modes occurred and included complex local damages, the maximum load might not be readily available. In order to predict the strength of the panels failed in various modes, finite element analysis was conducted. Additionally, the influences of the two damages, core shear crack and indentation, were demonstrated in Fig. 11. It is seen that the core shear crack could lead to a sudden drop of the load, while the indentation had two effects on the capacity: First, if the indentation resulted from the face yield, the area of indentation was limited, near the loading roller, and in this case the capacity had a sharp and large drop; Second, if the indentation resulted from the development of the plastic zone of the foam core, the area of indentation was greater at the loading roller, and the load slowly decreased as the indentation developed. As for the stiffness, it includes the bending and shear stiffness. The initial stiffness was used to study the effects of design parameters.

Fig. 12 presents the relationship between design parameters and mechanical characteristics. D3-30-20-A is selected as the control specimen. It was shown that the load-carrying capacity and stiffness of the panel increased as the density of foam core increased. The comparison between the curved and flat sandwich panels was also conducted. It is evident that the curved panel provides a higher stiffness than the flat. The load-carrying capacity of the flat panel, however, was much greater than that of the curved. This is due to the catenary action formed in the flat panel whose both ends were clamped. As for the core thickness. It is found that a higher capacity and stiffness was achieved as the thickness

of the core increased. Unsurprisingly, the load-carrying capacity and stiffness of the sandwich panel increased as more layers in 0° direction were provided.

4.3. Finite element analysis

4.3.1. Modeling

To assess the failure modes and further to carry out the parametric study, the finite element analysis (FEA) was conducted using MSC.Marc. MSC.Marc is able to solve the nonlinear problems involving large deformation and material nonlinearity. In the finite element model (FEM), 4-node quadrilateral thick shell element (75 # shell) was used to simulate GFRP face sheets and the 8-node hexahedral solid element (7 # solid) was used to simulate the foam core. The two elements shared the same nodes at the interface based on the full bond assumption. In order to reduce the computational cost, one half of structure was modeled, as shown in Fig. 13(a). In addition, a mesh convergence test was conducted through element refinement, and the element size was then determined.

The boundary conditions were determined by referring to the experimental setup. The two ends of the specimen were totally fixed. The load was directly applied to the nodes of the top face sheet. Additionally, a cylinder was built to simulate the loading roller and the load was applied to the nodes at the top of the cylinder, as shown in Fig. 13 (b). All the loads were applied in the manner of displacement-control.

The elastic-plastic compressive behavior and the tension crack of PU foam were considered. The von Mises yield surface and isotropic hardening criterion were adopted to define the elastic-plastic behavior. In particular, in the plastic behavior was determined by material characterization tests. The measured stress-equivalent plastic strain relationships are shown in Fig. 14, which could be obtained by deducing the elastic strain in the uniaxial stress-strain relationship. To consider the

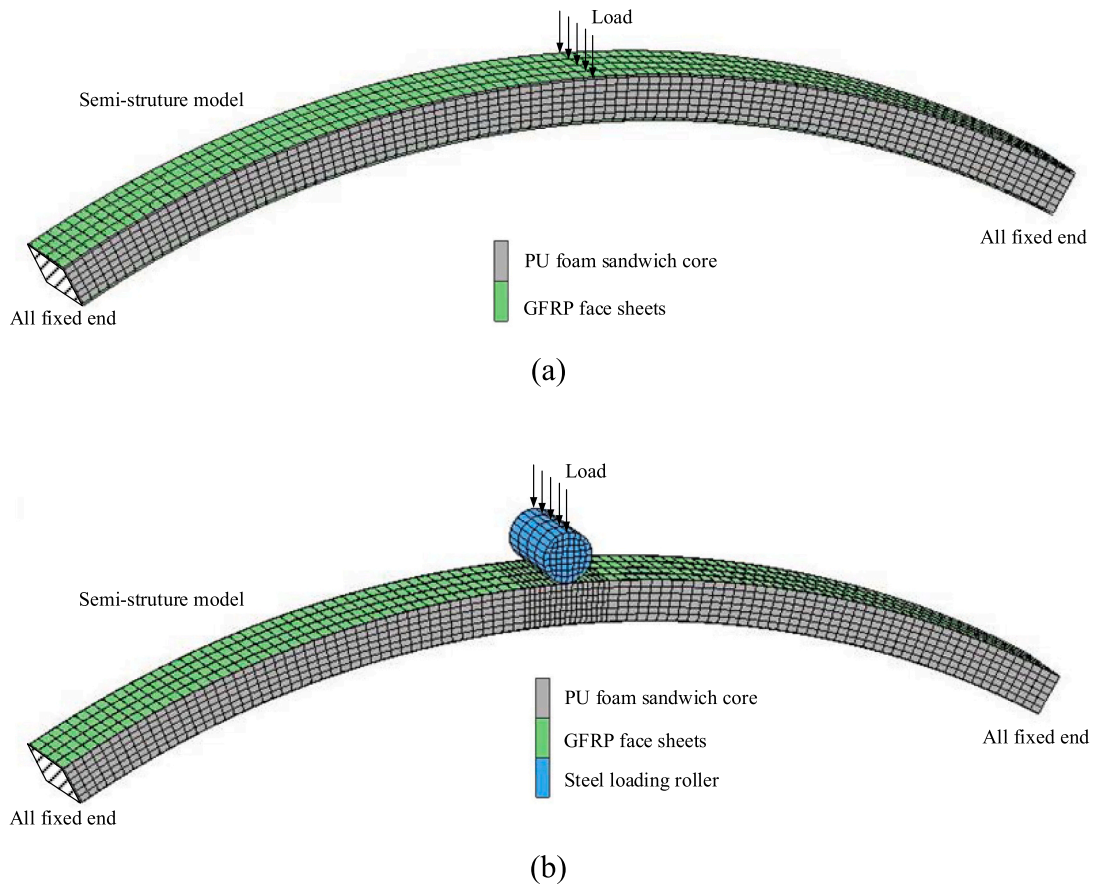


Fig. 13. Mesh and boundary conditions of FEM: (a) typical FEM mesh and (b) refined FEM mesh for specimen D3-30-20-B.

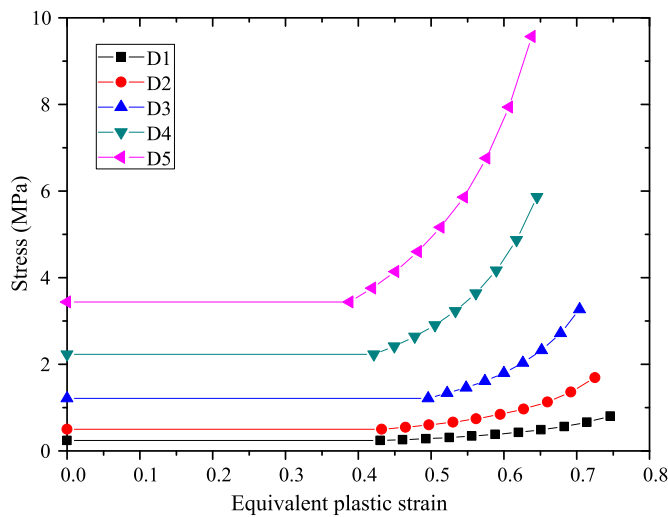


Fig. 14. Stress-equivalent plastic strain relationships of PU foam.

possible errors in experimental tests and achieve a conservative design, the design value of compressive yield strength was set as 0.92 of the experimental strength for specimens with a density of 125.6 kg/m³. It is noted that this strength factor cannot be directly applied to other specimens as these factors were not the same for all specimens with different densities. When defining the tension crack, the tensile strength was set as 0.85–0.87 of the experimental strength for specimens with a density of 125.6 kg/m³, and the softening modulus was set as 0.1 of the initial modulus. The crushing strain was set sufficiently large so as to avoid the crushing failure of the foam core. Additionally, the shear retention factor was set as 0.01 to simulate the brittle shear crack of the core.

4.3.2. Validation

The finite element model was validated by the experimental results, as shown in Table 5. In particular, the failure modes and the load-carrying capacities were compared and discussed.

It is seen that the modeling method has a good agreement with the experimental results, as shown in Fig. 15. For the failure mode CS, taking specimen D3-30-15-A for example, it could be found that the FEA accurately simulated the failure mode, and the predicted load-displacement curve agreed well with the experimental results. For the failure mode FC-INT-CS, the control specimen D3-30-20-A was chosen to conduct the simulation. The failure process, including face crushing, indentation and core shear crack, was successfully captured. The simulated curve also has a good agreement with the experimental results. The failure mode INT-CS was only observed on specimen D2-30-20-A. The factors defined in FEA were adjusted to avoid the premature

failure of GFRP face sheets due to the foam core with density of 77.6 kg/m³ (designated as D2) having a much larger shear deformation than other specimens having different densities. The compressive strength of GFRP face sheet was set as 250 MPa. The compressive and tensile strength of PU foam core was set as 1.1 and 0.65 times of the experimental results, respectively. The failure modes and the load-displacement relationships could be accurately simulated, as shown in Fig. 15(c). For failure mode INT-FW-CS, the loading roller was built and the contact elements were used to achieve a better simulation. The simulated curve was shown in Fig. 15(d). It is found that the indentation could be simulated, though the load was higher than the experimental result. Additionally, the face wrinkle cannot be simulated without considering initial imperfections.

4.3.3. Parametric study

Based on the proposed modeling method, a parametric study was conducted to address the influence of design parameters, including the inclined angle and the core thickness, on the failure mode and load-carrying capacity. The foam density and the stacking sequence were not considered in the parametric design due to the fact that the sound conclusion could be drawn through experimental results. The specimens were designated using the same rule as those in the experimental tests.

First, the inclined angle was varied from 0° to 90° by every 15°, namely from flat panel to semi-circle panel. The results are shown in Fig. 16(a). The flat panel has a different stress flow with other curved panels and thus, only a part of the load-displacement relationship is presented. It is found that the stiffness of the curved panels has uniformly greater stiffness than that of flat panel. The specimens with inclined angles of 30° and 45° show the greatest stiffness. The failure mode changed from FC-INT-CS to CS as the inclined angle increased. For the curved panels, the capacity increased at first and then remained stable.

Second, the thickness of the foam core was varied from 15 to 30 mm by every 5 mm. The results of FEA are shown in Fig. 16(b). It could be found that with the core thickness increasing, the stiffness of specimens increased. Additionally, the failure modes changed from CS to FC-INT-CS as the core thickness increased. The load-carrying capacity also increased with the core thickness increased. Nonetheless, the amplitude of such increase gradually became smaller as the indentation occurred.

5. Conclusions

In this work, an experimental test was conducted on the GFRP curved sandwich panels. A total of 12 panels were manufactured and tested to investigate the influences of the key design parameters on the load-carrying capacity and failure modes of the panel, including the foam density, inclined angle, core thickness and stacking sequence of the face sheet. In addition, finite element analysis was conducted to reveal the failure mechanism of the specimens. The following conclusions can be drawn from this work:

Table 5

Comparisons between the experimental and FEA results.

Specimens	Initial stiffness (kN/mm)			Maximum load (kN)			Failure mode	
	Test	FEA	Error (%)	Test	FEA	Error (%)	Test	FEA
D1-30-20-A	0.141	0.132	-6.38	0.567	0.601	6.00	CS	CS
D2-30-20-A	0.301	0.276	-8.31	1.260	1.242	-1.43	INT-CS	INT-CS
D3-30-20-A	0.564	0.547	-3.01	2.195	2.217	1.00	FC-INT-CS	FC-INT-CS
D4-30-20-A	0.819	0.748	-8.67	3.512	3.488	-0.68	FC-INT-CS	FC-INT-CS
D5-30-20-A	0.994	1.007	1.31	3.968	3.828	-3.53	INT-FW-CS	INT-CS
D3-00-20-A	0.159	0.150	-5.66	6.065	7.838	29.23	FC-INT-CS	FC-INT-CS
D3-60-20-A	0.503	0.439	-12.72	2.176	2.257	3.72	CS	CS
D3-90-20-A	0.323	0.342	5.88	2.210	2.215	0.23	CS	CS
D3-30-15-A	0.472	0.457	-3.18	1.689	1.803	6.75	CS	CS
D3-30-20-B	0.424	0.380	-10.38	1.295	1.345	3.86	INT-FW-CS	INT-CS
D3-30-20-C	0.716	0.723	0.98	2.505	2.742	9.46	CS	CS
D3-30-20-D	0.767	0.742	-3.26	3.040	3.165	4.11	CS	CS

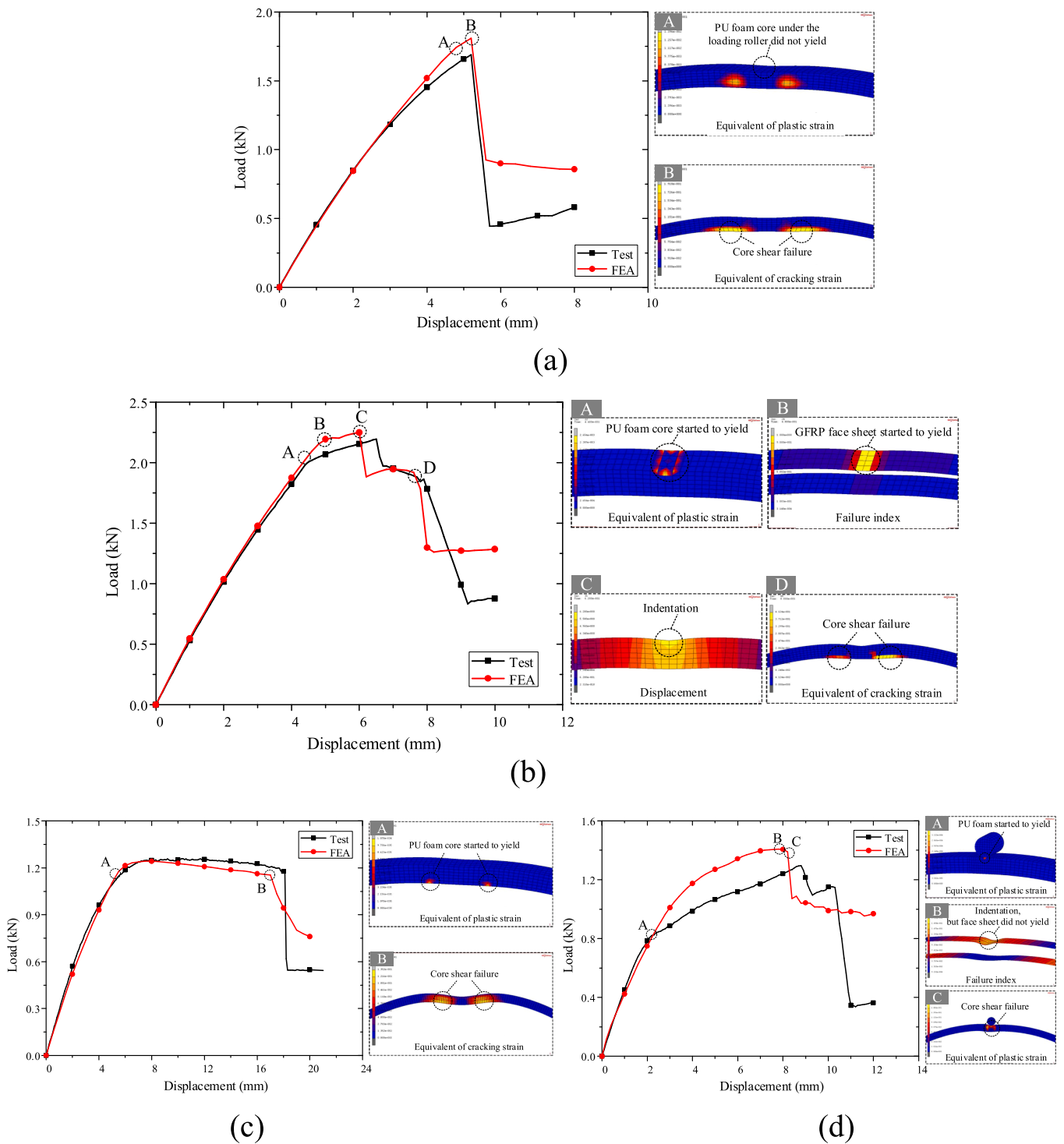
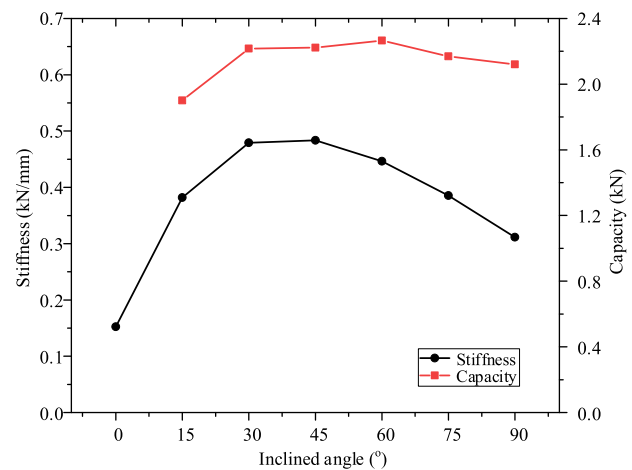
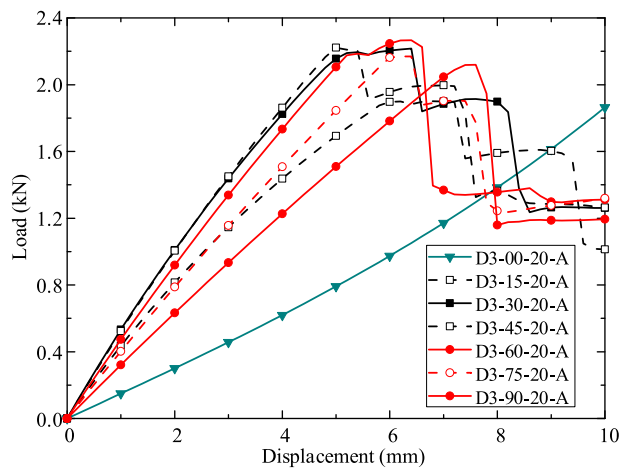


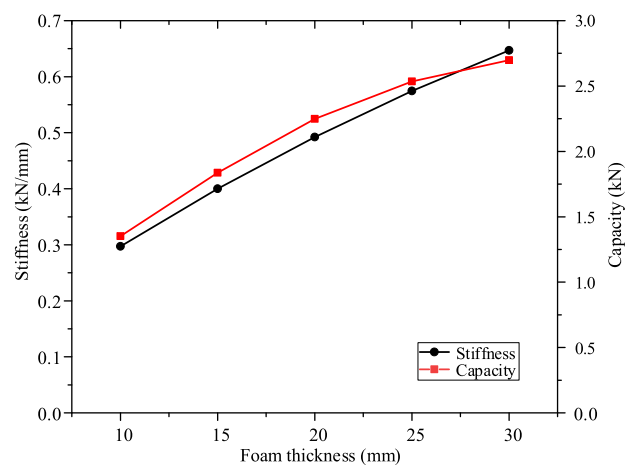
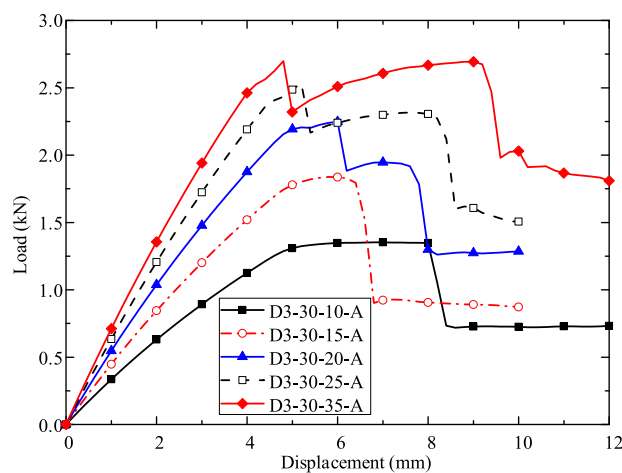
Fig. 15. Comparison of load-displacement curves at midspan between experimental and numerical results: (a) failure mode CS (specimen D3-30-15-A), (b) failure mode FC-INT-CS (specimen D3-30-20-A), (c) failure mode INT-CS (specimen D2-30-20-A) and (d) failure mode INT-FW-CS (specimen D3-30-20-B).

- (1) The singly curved GFRP sandwich panels exhibited four types of local damages, including core shear crack, face crushing, face wrinkle and indentation, which were identical to the flat panel. Additionally, four failure modes were identified, and each failure mode may consist of one or more local damages.
- (2) The singly curved sandwich arch showed an improved stiffness and small deformation. The stiffness of the curved panel, when inclined to 30°, was 250 % higher than that of the flat panel. An appropriate inclined angle is essential to achieve a high structural

- performance. However, the stress concentration due to concentrated load at the curved sandwich panel might lead to indentation and reduced capacity.
- (3) The strength and stiffness of the singly curved GFRP sandwich panel increased as the foam core density and the core thickness increased. In addition, the ply stacking sequence should be designed to carry the load directly, but the multidirectional-stacked ply is recommended to avoid the sheet splitting.



(a)



(b)

Fig. 16. Parametric study on behavior of curved panel: (a) inclined angle and (b) thickness of foam core.

- (4) A finite element model using MSC.Marc was proposed and validated through experimental results. The proposed model was found to have excellent accuracy in predicting the load-carrying capacity and the failure modes of the GFRP curved sandwich panel.

CRediT authorship contribution statement

TianQiao Liu: Writing – review & editing, Data curation. **Peng Feng:** Writing – review & editing, Supervision, Project administration, Funding acquisition, Conceptualization. **JiaQi Zhai:** Writing – review & editing, Investigation, Data curation. **Xinmiao Meng:** Writing – original draft, Project administration, Methodology, Investigation, Conceptualization. **Daobo Zhang:** Writing – review & editing, Validation, Investigation, Data curation.

Declaration of Competing Interest

The authors declare that they have no known competing financial interests or personal relationships that could have appeared to influence the work reported in this paper.

Data availability

Data will be made available on request.

Acknowledgments

The authors acknowledge fundings supported by the National Natural Science Foundation of China (No. U2106219), the Key Technologies R&D Program of CNBM (2021HX1617), and the XPLOER Prize.

References

- [1] Hu N, Feng P, Dai G-L. Structural art: past, present and future. *Eng Struct* 2014;79: 407–16. <https://doi.org/10.1016/j.engstruct.2014.08.040>.
- [2] Eigensatz M, Kilian M, Schiftner A, et al. Paneling architectural freeform surfaces. *Acm Trans Graph* 2010;29:1–10. <https://doi.org/10.1145/1778765.1778782>.
- [3] Adriaenssens S, Block P, Veenendaal D, et al. *Shell structures for architecture: form finding and optimization*. Routledge; 2014. <https://doi.org/10.4324/9781315849270>.
- [4] Pérez-Lombard L, Ortiz J, Pout C. A review on buildings energy consumption information. *Energy Build* 2008;40:394–8. <https://doi.org/10.1016/j.enbuild.2007.03.007>.
- [5] Lee BJ, Pessiki S. Thermal performance evaluation of precast concrete three-Wythe sandwich wall panels. *Energy Build* 2006;38:1006–14. <https://doi.org/10.1016/j.enbuild.2005.11.014>.
- [6] Nyers J, Komuves P. Optimum of external wall thermal insulation thickness using total cost method. In: *Proceedings of the Expres 2015, international symposium on exploitation of renewable energy sources and efficiency*; 2015.
- [7] Manalo A, Aravinthan T, Fam A, et al. State-of-the-art review on FRP sandwich systems for lightweight civil infrastructure. *J Compos Constr* 2016;21:04016068. [https://doi.org/10.1061/\(ASCE\)CC.1943-5614.0000729](https://doi.org/10.1061/(ASCE)CC.1943-5614.0000729).
- [8] Meng X, Feng P, Zheng Y. The application to bridge enclosure system of FRP curved sandwich panels with foam core. In: *Proceedings of the 6th Asia-Pacific conference on FRP in structures (APPIS2017)*. Singapore; 2017.

- [9] Zhao D, Liu TQ, Lu X, et al. Experimental and numerical analysis of a novel curved sandwich panel with pultruded GFRP strip core. *Compos Struct* 2022;288:115404. <https://doi.org/10.1016/j.compstruct.2022.115404>.
- [10] Chen C, Fang H, Zhu L, et al. Low-velocity impact properties of foam-filled composite lattice sandwich beams: experimental study and numerical simulation. *Compos Struct* 2023;306:116573. <https://doi.org/10.1016/j.compstruct.2022.116573>.
- [11] Bakis CE, Bank LC, Brown VL, et al. Fiber-reinforced polymer composites for construction-state-of-the-art review. *J Compos Constr* 2002;6(2):73–87. [https://doi.org/10.1061/\(ASCE\)1090-0268\(2002\)6:2\(73\)](https://doi.org/10.1061/(ASCE)1090-0268(2002)6:2(73)).
- [12] Teng JG, Chen JF, Smith ST, et al. FRP: strengthened RC structures. *Front Phys* 2002.
- [13] Fam A, Sharaf T. Flexural performance of sandwich panels comprising polyurethane core and GFRP skins and ribs of various configurations. *Compos Struct* 2010;92:2927–35. <https://doi.org/10.1016/j.compstruct.2010.05.004>.
- [14] Correia JR, Garrido M, Gonilha JA, et al. GFRP sandwich panels with PU foam and PP honeycomb cores for civil engineering structural applications. *Int J Struct Integr* 2012;3:127–47. <https://doi.org/10.1108/17579861211235165>.
- [15] Kendall D. Building the future with FRP composites. *Reinf Plast* 2007;51(26). [https://doi.org/10.1016/S0034-3617\(08\)70131-0](https://doi.org/10.1016/S0034-3617(08)70131-0) [31-29,33].
- [16] Meng X, Feng P, Huang S. Use of FRP in integrating multi-functional nonlinear architecture. *Fiber Reinf Plast/Compos* 2014 [(In Chinese)].
- [17] Blonder A, Grobman YJ. Design and fabrication with fibre-reinforced polymers in architecture: a case for complex geometry. *Archit Sci Rev* 2016;59:257–68. <https://doi.org/10.1080/00038628.2015.1020479>.
- [18] Castaneda E, Lauret B, Lirola J, et al. Free-form architectural envelopes: digital processes opportunities of industrial production at a reasonable price. *J Facade Des Eng* 2015;3:1–13. <https://doi.org/10.3233/FDE-150031>.
- [19] Roosenboom FG. Building the future with FRP composites (Master Thesis). Accessed by (<http://resolver.tudelft.nl/uuid:583e26ab-fbd9-44bc-ac86-7aa6cabd-cf55>).
- [20] Keller T, Haas C, Vallée T. Structural concept, design, and experimental verification of a glass fiber-reinforced polymer sandwich roof structure. *J Compos Constr* 2008;12:454–68. [https://doi.org/10.1061/\(ASCE\)1090-0268\(2008\)12:4\(454\)](https://doi.org/10.1061/(ASCE)1090-0268(2008)12:4(454)).
- [21] Keller T, Vassilopoulos AP, Manshadi BD. Thermomechanical behavior of multifunctional GFRP sandwich structures with encapsulated photovoltaic cells. *J Compos Constr* 2010;14:470–8. [https://doi.org/10.1061/\(ASCE\)CC.1943-5614.0000101](https://doi.org/10.1061/(ASCE)CC.1943-5614.0000101).
- [22] Xu W. Structural envelope. *Archit J* 2014;1–5 [(in Chinese)].
- [23] Meng X, Feng P, Zheng Y. The application to bridge enclosure system of FRP curved sandwich panels with foam core. In: Proceedings of the Asia-Pacific conference on FRP in structures (APFIS2017). Singapore; 2017.
- [24] Hause T, Librescu L. Doubly curved anisotropic sandwich panels: modeling and free vibration. *J Aircr* 2007;44:1327–36. <https://doi.org/10.2514/1.26990>.
- [25] Yurddaskal M, Ozmen U, Kir M, et al. The effect of foam properties on vibration response of curved sandwich composite panels. *Compos Struct* 2018;183:278–85. <https://doi.org/10.1016/j.compstruct.2017.03.059>.
- [26] Cunningham PR, White RG, Aglietti GS. Effects of various design parameters on the free vibration of doubly curved composite sandwich panels. *J Sound Vib* 2000;230:617–48. <https://doi.org/10.1006/jsvi.1999.2632>.
- [27] Wang Q, Cui X, Qin B, et al. A semi-analytical method for vibration analysis of functionally graded (FG) sandwich doubly-curved panels and shells of revolution. *Int J Mech Sci* 2017;134:479–99. <https://doi.org/10.1016/j.ijmecsci.2017.10.036>.
- [28] Hause T, Librescu L. Dynamic response of doubly-curved anisotropic sandwich panels impacted by blast loadings. *Int J Solids Struct* 2007;44:6678–700. <https://doi.org/10.1016/J.IJSOLSTR.2007.03.006>.
- [29] Lu G, Shen J. Mechanical response of curved sandwich panels subjected to blast loading. In: Proceedings of the 8th international conference on shock and impact loads on structures; 2009. p. 405–12.
- [30] Shen J, Lu G, Wang Z, et al. Experiments on curved sandwich panels under blast loading. *Int J Impact Eng* 2010;37:960–70. <https://doi.org/10.1016/j.ijimpeng.2010.03.002>.
- [31] Shen J, Lu G, Zhao L, et al. Response of curved sandwich panels subjected to blast loading. *J Perform Constr Facil* 2011;25:382–93. [https://doi.org/10.1061/\(ASCE\)CF.1943-5509.0000234](https://doi.org/10.1061/(ASCE)CF.1943-5509.0000234).
- [32] Qi C, Yang S, Yang LJ, et al. Dynamic response and optimal design of curved metallic sandwich panels under blast loading. *Sci World J* 2014;853681. <https://doi.org/10.1155/2014/853681>.
- [33] Yurddaskal M, Baba BO. The effect of curvature on the impact response of foam-based sandwich composite panels. *Steel Compos Struct* 2016;20:983–97. <https://doi.org/10.12998/scs.2016.20.5.983>.
- [34] Baba BO. Curved sandwich composites with layer-wise graded cores under impact loads. *Compos Struct* 2017;159:1–11. <https://doi.org/10.1016/j.compstruct.2016.09.054>.
- [35] Sun G, Zhang J, Li S, et al. Dynamic response of sandwich panel with hierarchical honeycomb cores subject to blast loading. *Thin-Walled Struct* 2019;142:499–515. <https://doi.org/10.1016/j.tws.2019.04.029>.
- [36] Mahadik Y, Potter K. Experimental investigation into the thermoelastic spring-in of curved sandwich panels. *Compos Part A: Appl Sci Manuf* 2013;49:68–80. <https://doi.org/10.1016/j.compositesa.2013.02.006>.
- [37] Mehar K, Panda SK, Mahapatra TR. Nonlinear frequency responses of functionally graded carbon nanotube-reinforced sandwich curved panel under uniform temperature field. *Int J Appl Mech* 2018;10:1850028. <https://doi.org/10.1142/S175882511850028X>.
- [38] Van Tung H. Nonlinear thermomechanical response of pressure-loaded doubly curved functionally graded material sandwich panels in thermal environments including tangential edge constraints. *J Sandw Struct Mater* 2018;20:974–1008. <https://doi.org/10.1177/1099636216684312>.
- [39] Frostig Y, Baruch M, Vilnay O, et al. High-order theory for sandwich-beam behavior with transversely flexible core. *J Eng Mech* 1992;118:1026–43.
- [40] Skvortsov V, Bozhevolnaya E. Overall behaviour of shallow singly-curved sandwich panels. *Compos Struct* 1997;37:65–79. [https://doi.org/10.1016/S0263-8223\(97\)80004-9](https://doi.org/10.1016/S0263-8223(97)80004-9).
- [41] Skvortsov V, Bozhevolnaya E, Kildegaard A. Assessment of models for analysis of singly-curved sandwich panels. *Compos Struct* 1998;41:289–301. [https://doi.org/10.1016/S0263-8223\(98\)00048-8](https://doi.org/10.1016/S0263-8223(98)00048-8).
- [42] Skvortsov V, Bozhevolnaya E, Kildegaard A. Overall behaviour of singly curved shallow sandwich panels: the case of general boundary conditions. *Compos Struct* 2000;49:95–109. [https://doi.org/10.1016/S0263-8223\(99\)00129-4](https://doi.org/10.1016/S0263-8223(99)00129-4).
- [43] Afshin M, Sadighi M, Shakeri M. Static analysis of cylindrical sandwich panels with a flexible core and laminated composite face sheets. *J Compos Mater* 2010;44(12):1455–76. <https://doi.org/10.1177/00219983093592>.
- [44] Pope GG. The buckling behaviour in axial compression of slightly-curved panels, including the effect of shear deformability. *Int J Solids Struct* 1968;4:323–40. [https://doi.org/10.1016/0020-7683\(68\)90041-3](https://doi.org/10.1016/0020-7683(68)90041-3).
- [45] Davenport OB, Bert CW. Buckling of orthotropic, curved, sandwich panels in shear and axial compression. *J Aircr* 1973;10:632–4. <https://doi.org/10.2514/3.60271>.
- [46] Hause T, Librescu L, Camarda CJ. Postbuckling of anisotropic flat and doubly-curved sandwich panels under complex loading conditions. *Int J Solids Struct* 1998;35:3007–27. [https://doi.org/10.1016/S0020-7683\(97\)00360-0](https://doi.org/10.1016/S0020-7683(97)00360-0).
- [47] Gao Y, Hoo Fatt MS. Local facesheet pulse buckling in a curved, composite sandwich panel. *Compos Struct* 2013;104:249–60. <https://doi.org/10.1016/j.compstruct.2013.04.037>.
- [48] Hosseini M, Khalili SMR, Malekzadeh Fard K. An indentation law for doubly curved composite sandwich panels with rigid-plastic core subjected to flat-ended cylindrical indenters. *Compos Struct* 2013;105:82–9. <https://doi.org/10.1016/j.compstruct.2013.04.032>.
- [49] Kundu CK, Han JH. Nonlinear buckling analysis of hygrothermoelastic composite shell panels using finite element method. *Compos Part B: Eng* 2009;40:313–28. <https://doi.org/10.1016/j.compositesb.2008.12.001>.
- [50] Xiong J, Ghosh R, Ma L, et al. Bending behavior of lightweight sandwich-walled shells with pyramidal truss cores. *Compos Struct* 2014;116:793–804. <https://doi.org/10.1016/j.compstruct.2014.06.006>.
- [51] Xie H, Li W, Fang H, et al. Flexural behavior evaluation of a foam core curved sandwich beam. *Compos Struct* 2024;328:117729. <https://doi.org/10.1016/j.compstruct.2023.117729>.
- [52] Xie H, Hou X, Fang H, et al. Flexural behavior evaluation of PET foam core curved sandwich beam: experimental study and numerical simulation. *Constr Build Mater* 2024;414:135000. <https://doi.org/10.1016/j.conbuildmat.2024.135000>.
- [53] Lim TS. Failure modes of foam core sandwich beams under static and impact loads. *J Compos Mater* 2004;38:1639–62. <https://doi.org/10.1177/0021998304044760>.